Effective decay rates of nuclei in astrophysical environments[*]

Chao Dong (董超)[1] Zhi-Hong Li (李志宏)[1,2,3†] Ge-Xing Li (李歌星)[1] Yun-Ju Li (李云居)[1] Na Song (宋娜)[1]

Chen Chen (陈晨)[1] Jun-Wen Tian (田竣文)[1] Jia-Ying-Hao Li (李家英豪)[1] Zhi-Cheng Zhang (张智程)[1]

Hui-Ling Tian (田慧玲)[1] Mei-Yue-Nan Ma (马梅月楠)[1]

[1]China Institute of Atomic Energy, Beijing 102413, China
[2]University of Chinese Academy of Science, Beijing 101408, China
[3]Jinping Deep Underground Frontier Science and Dark Matter Key Laboratory of Sichuan Province, Liangshan 615000, China

Abstract: Nuclear β-decay plays a pivotal role at various stages of stellar evolution. However, the effective decay rates of nuclei in astrophysical environments may differ significantly from their laboratory values. This paper presents a detailed methodology for calculating nuclear half-life under the influence of temperature, electron density, ionization, and incomplete thermal equilibrium. We analyze the impact of astrophysical conditions on the β-decay of ^{26}Al, ^{59}Fe, ^{79}Se, and ^{205}Pb, revealing substantial variations in their effective half-lives within stellar environments. These changes lead to significant differences in nucleosynthetic yields, underscoring the critical importance of accounting for environmental effects when modeling nuclear decay rates.

Keywords: astrophysical environment, electron number density, thermal equilibrium, effective decay rate

I. INTRODUCTION

In nuclear astrophysics, the prediction of elemental abundance relies on incorporating nuclear reaction rates and decay rates into stellar models to simulate nucleosynthesis processes. This approach is fundamental for understanding the origin of elements in the universe. Nuclear β-decay plays a pivotal role at various stages of stellar evolution. Understanding nuclear decay rates in astrophysical environments is essential for unraveling the origins of elements in the universe. However, nuclear decay rates in stars can differ markedly from those observed on Earth.

Pioneering work by Cameron [1] demonstrated the importance of thermally populated excited states in enhancing decay rates. Specifically in stellar environments, nuclei are frequently excited by high-energy photons, leading to decay rates that differ significantly from those of ground states. Moreover, Bahcall [2] as well as Peterson and Bahcall [3] highlighted that elevated electron number density enhances electron-capture (EC) rates by supplying more high-energy electrons, while simultaneously suppressing β^- decay through Pauli blocking (occupied final electron states) [4]. Notably, in high-temperature ($T > 1$ $T_7(10^7$ K)) and high-density ($\rho > 10^3$ g/cm^3)

stellar interiors, elements undergo partial or complete ionization. As a result, the effective nuclear charge increases significantly, suppressing charge shielding effects. Furthermore, complete ionization eliminates bound-state electron capture (EC) due to the absence of orbital electrons. Most critically, ionization induced mass adjustments modify nuclear Q-values, enabling otherwise forbidden decays [5]. This effect is magnified for nuclei with laboratory measured β-decay Q-values that are small or marginally negative [6]. For example, the Q-value of β^- decay for fully ionized ^{205}Tl is 31.1(5) keV in the stellar interior, whereas the Q-value for its neutral atom is -50.6 keV under laboratory conditions.

Temperatures and densities can vary greatly in different nucleosynthesis environments. Therefore, stellar plasmas, where nucleosynthesis occurs, are not always fully ionized, and when thermodynamical conditions affect the ionization degree of the involved atoms, the β-decay process of their nuclei can also be strongly modified. Such an effect was first shown in the seminal work by Takahashi and Yokoi published in 1987 [7]; after 35 years, these values are still the most used in calculations of stellar and primordial nucleosynthesis. It is assumed that the initial nuclear states are in thermal equilibrium. The as-

sumption of instantaneous thermal equilibrium may fail for nuclei exhibiting metastable isomers [7], such as ^{26}Al, and internal γ transitions from the isomer (0^+) to the ground state (5^+) are inhibited by the large spin difference. Here, equilibration between isomeric and ground states occurs indirectly via intermediate levels [8]. Ward and Fowler [8] proposed a generalized framework for multi-level equilibration. However, their model neglects the critical effects of ionization degree and electron number density, which dominate in high-temperature stellar plasmas.

This study established a unified computational framework for β-decay rates in astrophysical environments, explicitly integrating four critical parameters: temperature (T), electron number density (n_e), ionization states, and nonthermal equilibrium corrections. The effective decay rates of ^{59}Fe, ^{79}Se, and ^{205}Pb were calculated using the latest experimental data.

II. METHODOLOGY

In stellar environments, nuclei are frequently excited by high-energy photons, leading to the population of low-lying excited states, as illustrated in Fig. 1. The evolution of the abundance between the excited states is described by the following equations [9]:

$$\frac{dn_m}{dt} = -\lambda_{mo}n_m + \lambda_{om}n_o - \lambda_m^\beta n_m, \tag{1}$$

$$\frac{dn_o}{dt} = \lambda_{mo}n_m - \lambda_{om}n_o - \lambda_o^\beta n_o. \tag{2}$$

The subscripts m and o indicate the excited and ground states, respectively. n is the abundance of the level. λ_m^β represents the β-decay rate of level m. λ_{mo} represents the γ transition from level m to level o, which consists of spontaneous transitions and is stimulated by photons; it is expressed as

$$\lambda_{mo} = \frac{\lambda_{mo}^s}{1 - e^{-(E_m - E_o)/kT}}, \tag{3}$$
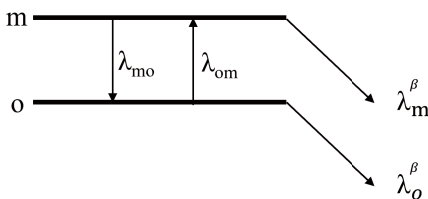
where λ_{mo}^s represents the spontaneous γ transition from

level o to level m. T is temperature, k_B is the Boltzmann constant, and E is the energy of the nuclear level. λ_{om} represents the induced transition from level o to level m and is expressed as

$$\lambda_{om} = \frac{G_m}{G_o} \frac{\lambda_{mo}^s}{e^{(E_m - E_o)/kT} - 1}, \tag{4}$$

where G is the partition function of nuclear level. For the case of internal equilibration, the abundance ratio of the two levels is given by

$$\frac{n_m}{n_o} = \frac{G_m \exp(-E_m/k_B T)}{G_m \exp(-E_m/k_B T) + G_o \exp(-E_o/k_B T)}. \tag{5}$$

The effective decay rate λ is derived from the weighted average of the β-decay rates at different nuclear levels [7, 10]:

$$\begin{aligned} \lambda &= \sum_K P_K \cdot \lambda_K^\beta \\ &= \frac{G_K \exp(-E_K/k_B T) \cdot \lambda_K^\beta}{\sum_K G_K \exp(-E_K/k_B T)}, \end{aligned} \tag{6}$$

where the subscript K represents the nuclear level. P_K is the layout probability at thermal equilibrium. λ_K and E_K are the decay rate and energy, respectively. T is temperature.

In some cases, internal γ transitions from the isomer to the ground state are inhibited by the large spin difference, necessitating equilibration through an intermediate state, as illustrated in Fig. 2. The evolution of the abundance between the three levels for the nuclei is expressed as

$$\frac{dn_j}{dt} = -\lambda_{jo}n_j - \lambda_{jm}n_j - \lambda_j^\beta n_j + \lambda_{oj}n_o + \lambda_{mj}n_m, \tag{7}$$

$$\frac{dn_m}{dt} = -\lambda_{mo}n_m + \lambda_{jm}n_j - \lambda_m^\beta n_m + \lambda_{om}n_o - \lambda_{mj}n_m, \tag{8}$$
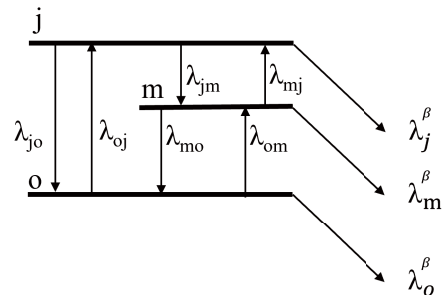

Fig. 1. Internal equilibration of a single excited state and the ground state of a nucleus.

Fig. 2. Internal equilibration of a three-level nuclear system.

$$\frac{\mathrm{d}n_o}{\mathrm{d}t} = \lambda_{jo}n_j + \lambda_{mo}n_m - \lambda_o^\beta n_o - \lambda_{oj}n_o - \lambda_{om}n_o. \tag{9}$$

Ward and Fowler [8] provided general numerical calculations for this case. The rates of change of the abundances n of the nuclear levels can be writen by the coupled set of first order differential equations in matrix form as

$$\frac{\mathrm{d}}{\mathrm{d}t}\boldsymbol{N} = \boldsymbol{T} \cdot \boldsymbol{N}, \tag{10}$$

where $\boldsymbol{T}$ is the β-decay and internal electromagnetic transition matrix [8] that follows from Eqs. (7)–(9), and

$$\boldsymbol{N} = \begin{Bmatrix} n_o(t) \\ n_m(t) \\ n_j(t) \end{Bmatrix}. \tag{11}$$

The general solution to this equation is of the form

$$N(t) = \sum_i N_i \mathrm{e}^{-\lambda_i t} \tag{12}$$

where N_i and $-\lambda_i$ are the eigenvectors and eigenvalues of $\boldsymbol{T}$, respectively. By definition, the effective decay rate λ is expressed as

$$\lambda = \frac{\sum_i N_i \lambda_i \mathrm{e}^{-\lambda_i t}}{N(t)}. \tag{13}$$

At the temperature of interest, for a sufficiently long time, if $\lambda_3 \ll \lambda_2$ and $\lambda_3 \ll \lambda_1$, the effective decay rate $\lambda \approx \lambda_3$.

Meanwhile, in the stellar environment, the nuclei may have different ionizations, such as bare nuclei, incompletely ionized atoms, and neutral atoms. λ_K is derived from the weighted average of decay rates at different ionization as follows [7]:

$$\begin{aligned} \lambda_K &= \sum_r P_r \lambda_{K,r} \\ &= \frac{\sum_r N_r \lambda_{K,r}}{\sum_r N_r}, \end{aligned} \tag{14}$$

where the subscripts r and $r+1$ represent r-times and $r+1$-times ionized, respectively. N_r and P_r are the abundance and probability of the ion, respectively. The ionization probability of atoms in the stellar environment can be obtained from the Saha ionization equation [11]:

$$\frac{N_{r+1}}{N_r} = \frac{2b_{r+1}}{2b_r} \frac{(2\pi k_B T)^{(3/2)}}{h^3} e^{-\frac{I_r}{k_B T}}, \tag{15}$$

where b_r is the partition function of the r-times ionized atom, h is Planck's constant, and I_r is the ionization potential. In addition, electrons in an atom or ion can also be thermally excited in the same way as nucleons. $\lambda_{K,r}$ is given by the following equation [7]:

$$\begin{aligned} \lambda_{K,r} &= \sum_k P_k \lambda_{K,r,k} \\ &= \frac{\sum_k g_k \exp(-e_k/k_B T)\lambda_{K,r,k}}{\sum_k g_k \exp(-e_k/k_B T)} \end{aligned} \tag{16}$$

where the subscript k is the level of the atom or ion. g is the partition function of the ion. $\lambda_{K,r,k}$ is given by the following equation [7]:

$$\lambda_{K,r,k} = \frac{\ln 2}{ft} \cdot f_m, \tag{17}$$

where m=a, 1nu, 1u, and 2u represent allowed, non-unique first-forbidden, unique first-forbidden, and unique second-forbidden transitions, respectively. ft is the comparative half-life. For free electrons (positrons) to be emitted or captured, f_m is the phase space integral, given by [4, 12−14]

$$\begin{aligned} f_m^{ec} = &\int_{W_{\min}}^\infty W\sqrt{W^2-1}(Q_{ij}+W)^2 F_0(Z,W)S_m(Z,W) \\ &G_e(W)(1-G_\nu(Q_{ij}+W))\mathrm{d}W\,, \end{aligned} \tag{18}$$

$$\begin{aligned} f_m^{\beta^+} = &\int_1^{Q_{ij}} W\sqrt{W^2-1}(Q_{ij}-W)^2 F_0(-Z+1,W) \\ &S_m(-Z+1,W)(1-G_p(W))(1-G_\nu(Q_{ij}-W))\mathrm{d}W, \end{aligned} \tag{19}$$

$$\begin{aligned} f_m^{\beta^-} = &\int_1^{Q_{ij}} W\sqrt{W^2-1}(Q_{ij}-W)^2 F_0(Z+1,W) \\ &S_m(Z+1,W)(1-G_e(W))(1-G_\nu(Q_{ij}-W))\mathrm{d}W, \end{aligned} \tag{20}$$

$$\begin{aligned} f_m^{pc} = &\int_{W_{\min}}^\infty W\sqrt{W^2-1}(Q_{ij}+W)^2 F_0(-Z,W)S_m(-Z,W) \\ &G_p(W)(1-G_\nu(Q_{ij}+W))\mathrm{d}W, \end{aligned} \tag{21}$$

where W is the total, rest mass, and kinetic energy of the electron or positron in units of $m_e c^2$. Z is the proton number of the parent nucleus. Q_{ij} is the decay energy between

the initial state of the parent i and final state of the daughter j in units of $m_e c^2$. $W_{\min}$ is the lowest energy of the electron (positron) in the β-decay in units of $m_e c^2$:

$$W_{\min} = \begin{cases} 1, & \text{for } Q_{ij} \geq -1, \\ |Q_{ij}|, & \text{for } Q_{ij} < -1, \end{cases} \tag{22}$$

$F(Z, W)$ is the Fermi function [14−17]:

$$F(Z, W) = \begin{cases} F_0(Z, W), & \text{for } m = \text{a, 1nu,} \\ F_1(Z, W), & \text{for } m = \text{1u,} \\ F_2(Z, W), & \text{for } m = \text{2u,} \end{cases} \tag{23}$$

where

$$F_0(Z, W) = 4 \frac{\left| \Gamma\left(\sqrt{1 - \alpha^2 Z^2} + i \frac{\alpha Z W}{\sqrt{W^2 - 1}} \right) \right|^2}{|\Gamma(1 + 2\sqrt{1 - \alpha^2 Z^2})|^2}$$
$$\times (2R\sqrt{W^2 - 1})^{2(\sqrt{1 - \alpha^2 Z^2} - 1)} \exp\left(\frac{\pi \alpha Z W}{\sqrt{W^2 - 1}} \right), \tag{24}$$

$$F_1(Z, W) = (4!)^2 \frac{\left| \Gamma\left(\sqrt{4 - \alpha^2 Z^2} + i \frac{\alpha Z W}{\sqrt{W^2 - 1}} \right) \right|^2}{|\Gamma(1 + 2\sqrt{4 - \alpha^2 Z^2})|^2}$$
$$\times (2R\sqrt{W^2 - 1})^{2(\sqrt{4 - \alpha^2 Z^2} - 2)} \exp\left(\frac{\pi \alpha Z W}{\sqrt{W^2 - 1}} \right), \tag{25}$$

and

$$F_2(Z, W) = (6!)^2 \frac{\left| \Gamma\left(\sqrt{9 - \alpha^2 Z^2} + i \frac{\alpha Z W}{\sqrt{W^2 - 1}} \right) \right|^2}{4|\Gamma(1 + 2\sqrt{9 - \alpha^2 Z^2})|^2}$$
$$\times (2R\sqrt{W^2 - 1})^{2(\sqrt{9 - \alpha^2 Z^2} - 3)} \times \exp\left(\frac{\pi \alpha Z W}{\sqrt{W^2 - 1}} \right), \tag{26}$$

where $\alpha \approx \frac{1}{137}$ is the fine structure constant, Γ is the gamma function, and R is the nuclear radius in units of $\hbar/mc$. $S_m(Z, W)$ are the spectral shape factors [13, 15, 16]:

$$S_m(Z, W) = \begin{cases} L_0 & \text{for } m = \text{a, 1nu,} \\ (W_v)^2 L_0 + 9L_1 & \text{for } m = \text{1u,} \\ (W_v)^4 L_0 + 30L_1(W_v)^2 + 225L_2 & \text{for } m = \text{2u,} \end{cases} \tag{27}$$

where W_v is the neutrino energy in units of $m_e c^2$. L_0, L_1, and L_2 are certain combinations of electron radial wave functions evaluated at an appropriately chosen nuclear radius R [13, 15, 16, 18]:

$$L_0 = \frac{1 + \sqrt{1 - \alpha^2 Z^2}}{2}, \tag{28}$$

$$L_1 = \frac{F_1(Z, W)}{F_0(Z, W)} \frac{W^2 - 1}{9} \frac{2 + \sqrt{4 - \alpha^2 Z^2}}{4}, \tag{29}$$

and

$$L_2 = \frac{F_2(Z, W)}{F_0(Z, W)} \frac{(W^2 - 1)^2}{225} \frac{3 + \sqrt{9 - \alpha^2 Z^2}}{6}. \tag{30}$$

The last two terms of the phase space integal f_m are related to the electron, positron, and neutrino distributions. G_e, G_p, and G_v are the Fermi–Dirac distribution functions of the electron, positron, and neutrino:

$$G_e = \frac{1}{1 + e^{\frac{E_e - U_F}{kT}}}, \tag{31}$$

$$G_p = \frac{1}{1 + e^{\frac{E_p + U_F}{kT}}}, \tag{32}$$

$$G_v = \frac{1}{1 + e^{\frac{E_v}{kT}}}, \tag{33}$$

where E_e, E_p, and E_v are the energies of the electron, positron, and neutrino in units of MeV, respectively. U_F is the Fermi energy of the electrons in units of MeV. The relation between Fermi energy and electron number density is given by [4, 13]

$$\rho Y_e = \frac{(m_e c)^3}{\pi^2 \hbar^3 N_A} \int_1^\infty W\sqrt{W^2 - 1}(G_e - G_p) dW. \tag{34}$$

The chemical potential of the electron for given values ρY_e and T can be obtained by iterating Eqs. (31), (32), and (34).

For the bound-state β^- decay and bound-state (orbital) e^- capture processes, f_m is the lepton phase volume part, given by [17, 19]

$$f_m = \sum_x \sigma_x(\pi/2) \left[f_x \text{or } g_x \right]^2 Q_{ij}^2 S_{(m),x}, \tag{35}$$

where σ_x describes the vacancy (for bound-state β^- de-

cays) or occupancy (for orbital e$^-$ captures) of the electron orbit x and lies between zero and unity. $[g_x$ or $f_x]$ is understood to be the larger component of the electron radial wave functions evaluated at nuclear radius R, which can be obtained by RADIAL with self-consistent method [20]. Here, $S_{(m)x}$ are the spectral shape factors, given by [17, 19]

$$S_{(m),x} = \begin{cases} 1 & \text{for } m = \text{a}, 1\text{nu} \text{ and } x = n\text{s}_{1/2}, n\text{p}_{1/2} \\ Q_{ij}^2 & \text{for } m = 1\text{u} \text{ and } x = n\text{s}_{1/2}, n\text{p}_{1/2} \\ \dfrac{9}{R^2} & \text{for } m = 1\text{u} \text{ and } x = n\text{p}_{3/2}, n\text{d}_{3/2} \\ 0 & \text{otherwise} \end{cases} . \quad (36)$$

III. EFFECTIVE DECAY RATES OF ^{26}Al, ^{59}Fe, ^{79}Se, AND ^{205}Pb IN STELLAR INTERIOR

Having established the methodology for calculating the effective decay rates, we now present the results obtained under various astrophysical conditions.

In β^+-decays, contributions from continuum and orbital electron capture processes are included, while in β^--decays, those from the bound state β^- processes are taken into account.

A. ^{26}Al

The nucleosynthesis of the observable long-lived radioactive nuclides ^{26}Al ($T_{1/2} = 0.717$ Myr) and ^{60}Fe ($T_{1/2} = 2.26$ Myr) is an important constraint on stellar models [21]. The abundances inferred from γ-ray astronomy may have important implications for rotationally induced mixing, convection theory, mass loss theory, the initial mass function for massive stars, and the distribution of metals in the Galaxy [22].

However, the predicted yield ratio ^{60}Fe/^{26}Al is larger than the experimental value [21]. Studies have shown that the main source of theoretical prediction uncertainty is the reaction cross section of the generation and destruc-

tion of these isotopes. The Log ft values of ^{26}Al and ^{59}Fe are listed in Tables 1 and 2, respectively. Therefore, to constrain the yield ratio ^{60}Fe/^{26}Al, it is necessary to calculate the decay rate. Internal γ transitions from the isomer (0^+) to the ground state (5^+) of ^{26}Al are inhibited by the large spin difference. Thus, thermal equilibrium cannot be established between the ground state and first excited state, but it can be achieved through an intermediate state [8, 9, 23]. The γ decay rates of ^{26}Al (internal) are listed in Table 3.

In this case, the method of Runkle [23] is used to describe the internal behavior of the system (equilibration) at high temperatures. The evolution of the clusters can be written as

$$\frac{\mathrm{d}}{\mathrm{d}t}(1 + c_{20}n_0) = -n_o[\lambda_o^\beta + c_{20}(\lambda_{2m} + \lambda_{23} + \lambda_2^\beta)] + n_m(\lambda_{m2} + c_{3m}\lambda_{32}), \quad (37)$$

$$\frac{\mathrm{d}}{\mathrm{d}t}(1 + c_{3m}n_m) = -n_m[\lambda_m^\beta + \lambda_{m2} - c_{3m}(\lambda_{32} + \lambda_3^\beta)] + n_0c_{20}(\lambda_{2m} + \lambda_{23}). \quad (38)$$

where the subscripts o, m, 2, and 3 refer to the ground state, isomer, 417 keV, and 1058 keV states, respectively. The β decay rates λ^β for each level are obtained by Eqs. (15)–(36), which are different from those of Runkle [9, 23] in that the effects of electron number density, chemical potential, and ionization are ignored. The factors c_{ij} are the thermal equilibrium abundance c_{ij} ratios

$$c_{ij} = \frac{G_i}{G_j}\mathrm{e}^{-(E_i - E_j)/kT}. \quad (39)$$

This can be recast as a matrix equation

Table 2. Log ft values for the decay of ^{59}Fe$\rightarrow^{59}$Co.

Transitions	Log ft
g.s.$\rightarrow$1.099 MeV	6.7 [24]
g.s.$\rightarrow$1.292 MeV	5.98 [24]
0.473 MeV$\rightarrow$g.s.	5.41 [21]
0.571 MeV$\rightarrow$g.s.	5.55 [21]

Table 3. Electromagnetic transition rates of ^{26}Al [23].

Transitions	Multipolarity	$\lambda(s^{-1})$
0.417 MeV$\rightarrow$g.s.	E2	6.88×10^8
0.417 MeV$\rightarrow$228 MeV	M3	0.062
1.058 MeV$\rightarrow$417 Mev	E2	7.24×10^8

Table 1. Log ft values for the decay of ^{26}Al$\rightarrow^{26}$Mg [4].

Transitions	Log ft
g.s.$\rightarrow$1.809 MeV	14.18
g.s.$\rightarrow$2.938 MeV	13.35
0.228 MeV$\rightarrow$g.s.	3.48
0.417 MeV$\rightarrow$1.809 MeV	3.63
0.417 MeV$\rightarrow$2.938 MeV	4.66
1.058 MeV$\rightarrow$g.s. MeV	4.01
1.058 MeV$\rightarrow$1.809 MeV	3.36
1.058 MeV$\rightarrow$2.938 MeV	4.63

$$\frac{\mathrm{d}}{\mathrm{d}t} \boldsymbol{N} = \boldsymbol{T} \cdot \boldsymbol{N}, \tag{40}$$

where $\boldsymbol{T}$ is the transition matrix that follows from Eqs. (37) and (38), and

$$\boldsymbol{N} = \begin{Bmatrix} (1 + c_{2o})n_o(t) \\ (1 + c_{3m})n_m(t) \end{Bmatrix}. \tag{41}$$

The smaller eigenvalues λ of $\boldsymbol{T}$ are related to the effective decay rate of ^{26}Al [23].

The effective decay rate of ^{26}Al is depicted in Fig. 3, illustrating the significant impacts of temperature and electron number density on its decay behavior. As the electron number density increases, the chemical potential of electrons rises, leading to an enhancement in the electron capture decay rate. The electron density dependence of positron emission is negligible in most cases of interest. With an increase in temperature, the decay rate of electron capture increases significantly owing to the increase in the contribution of excited states. At temperatures between 0.2 T_9 and 0.4 T_9, the decay rate exhibits
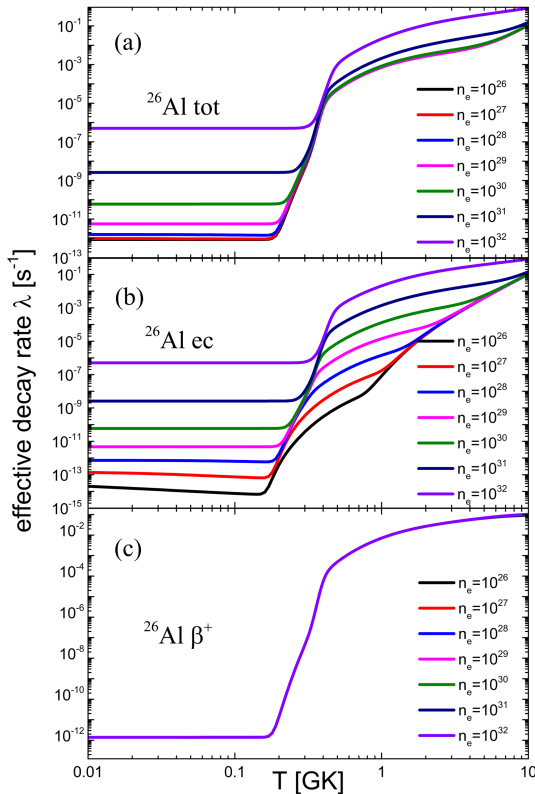
minimal dependence on the electron number density. This is because the thermal layout rate from ground state population to the first excited state is smaller than the β-decay rate of the first excited state at lower temperatures. In this case, the actual decay rate of the first excited state will be determined by its thermal layout rate, which is independent of electron number density. As the temperature continues to increase, the thermal equilibrium rate begins to exceed the β-decay rate. At this point, the interior of the nucleus can reach thermal equilibrium so that the effective decay rate of the nucleus is not restricted by the thermal layout rate. When incomplete thermal equilibrium is considered, the effective decay rate of the nuclei is smaller than the thermal equilibrium because of the restriction of the thermal layout rate at lower temperatures. Our calculations show that the effective decay rate is amplified by a factor of 10^{10} when the effects of the celestial environment are taken into account. This has a significant effect on the production of ^{26}Al in the star.

B.　^{59}Fe

As mentioned above, to constrain the yield ratio ^{60}Fe/^{26}Al, Gao *et al.* [21] measured the $B(GT)$ of the low excited state of ^{59}Fe to calculate the effective β^--decay rates and showed that the ^{60}Fe production yield of an 18 solar mass star by ^{59}Fe(n, γ) reaction is decreased significantly by 40%. However, the effect of electron number density and ionization was ignored in their research. To study the yield of ^{60}Fe, it is necessary to consider the environmental impact more comprehensively.

The effective decay rate of ^{59}Fe is calculated by considering the influences of temperature, electron number density, and ionization, as shown in Fig. 4. With an increase in temperature, the decay rate of ^{59}Fe increases by up to 1000 times. In contrast, the decay rates decrease with increasing environmental electron density. When the electron number density is 10^{30}, the effective decay rate is reduced by a factor of 10. When the electron number
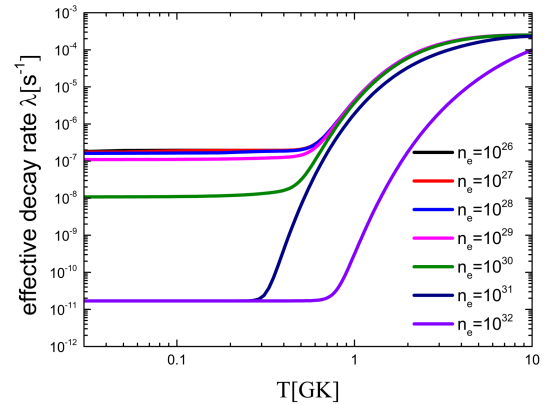

Fig. 3. (color online) Effective decay rate of ^{26}Al as a function of T and n_e. (a) Effective total decay rate λ_{tot} of ^{26}Al as a function of T and n_e. (b) Effective electron capture decay rate λ_{ec} of ^{26}Al as a function of T and n_e. (c) Effective decay rate λ_{β^+} of ^{26}Al as a function of T and n_e.

Fig. 4. (color online) Effective β^- decay rate λ_{β^-} of ^{59}Fe as a function of T and n_e.

density n_e is greater than 10^{29}, the effective decay rate of ^{59}Fe is significantly reduced. This leads to an increase in the production of ^{60}Fe in the stellar interior.

C. ^{79}Se

^{79}Se is a branching point in the slow neutron capture process (s-process), with relevant implications in nucleosynthesis and stellar models. The products of the s-process nucleosynthesis after ^{79}Se are the s-only isotopes ^{80,82}Kr, whose solar system abundances are accurately known. The Log ft value of ^{79}Se is listed in Table 4. The ground state half-life of ^{79}Se is 0.327 My, and its first excited state is 2 h. Therefore, the half-life of ^{79}Se is sensitive to the temperature of the stellar interior. This information, in conjunction with the decay rate of ^{79}Se, allows one to extract reliable conditions for temperature and neutron and electron number densities. The effective decay rate of ^{79}Se was given by Takahashi and Yokoi in 1987 [7]. However, the ground state of ^{79}Se was missing from their calculations, and the decay rates of the first excited and ground states were updated.

The effective decay rate of ^{79}Se was obtained using the latest data, as shown in Fig. 5. The effective decay rate of ^{79}Se is very sensitive to temperature. As the temperature rises, the effective decay rate of ^{79}Se increases by five orders of magnitude. In contrast, the decay rates decrease with increasing environmental electron density. In summary, the effective decay rate in the environment of interest is significantly greater than that on earth. This results in a lower yield ratio of ^{82}Kr/^{80}Kr. This is of great significance to the study of the s-process.

D. ^{205}Pb

As a unique pure s-process nucleus, ^{205}Pb can be used not only as a unique nucleosynthesis tracer but also as a ^{205}Pb-^{205}Tl clock to time the evolution of elements [26]. In conclusion, ^{205}Pb provides a unique opportunity to study s-process nucleosynthesis, which has important implications for the study of cosmic evolution and solar system formation. This was analyzed by Dong *et al.* [27], and the origin of ^{205}Pb in the solar system was investigated. At the temperature of interest, the layout probability P_K of the first excited state of ^{205}Pb is relatively large, as shown in Fig. 6. The decay rate of the first excited state (2.32 keV) is much greater than that of the ground state for this isotope. Thus, the effective decay rate of ^{205}Pb is very sensitive to temperature. Meanwhile, the higher electron number density can greatly increase the electron capture rate in the stellar interior. To obtain the yield of ^{205}Pb, it becomes crucial to calculate the effective decay rate of ^{205}Pb. In 2024, Leckenby [28] measured the bound-state β^- decay of ^{205}Tl to determine the Log ft value of the first excited state of ^{205}Pb, which further constrained the uncertainty brought by the input.

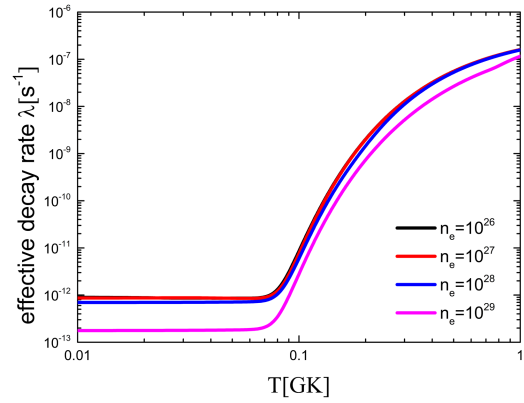The ionization probability P_r of ^{205}Pb obtained using

Fig. 5. (color online) Effective β^- decay rate λ_{β^-} of ^{79}Se as a function of T and n_e.
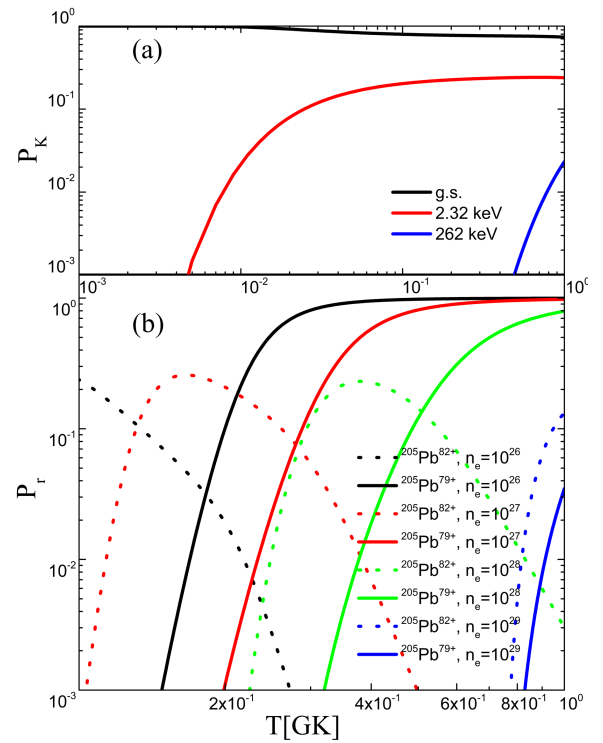

Fig. 6. (color online) Thermally populated probability P_K and ionization probability P_r as functions of T and n_e. (a) Thermally populated probability P_K of ^{205}Pb as a function of T and n_e. (b) Ionization probability P_r of ^{205}Pb as a function of T.

the Saha equation varies with temperature and density, as shown in Fig. 6. The ionization probabilities of ^{205}Pb^{82+} and ^{205}Pb^{79+} in different environments are shown. In the celestial environment of interest, ^{205}Pb^{82+} is the main component, in addition to a large number of highly ionized states. When the temperature is $0.1\ T_9 - 0.3\ T_9$, there is a large amount of highly ionized ^{205}Pb. In this case, orbital electron capture significantly increases the decay rate.

The latest data in Table 5 were used to calculate the effective decay rate of ^{205}Pb, as shown in Fig. 7. As the
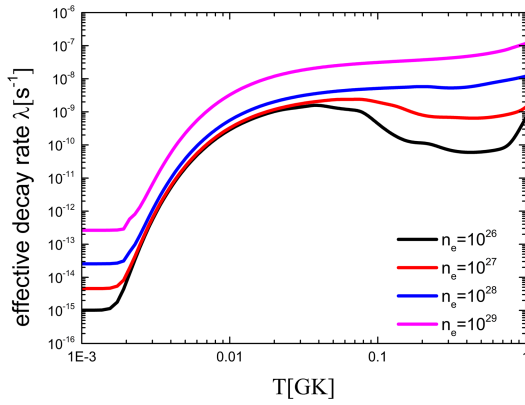
Fig. 7. (color online) Effective electron capture decay rate λ_{ec} of ^{205}Pb as a function of temperature and electron number density.

temperature increases, the decay rate of ^{205}Pb increases by a factor of 10^8. With an increase in temperature, the thermal distribution probability of the first excited state of 2.32 keV increases, and the decay rate becomes faster. The decay rate of ^{205}Pb from temperatures of 0.002 to 0.05 T_8 are enhanced significantly by the thermal population of the first excited state. Above 0.05 T_8, the rate decreases owing to increasing ionization, which reduces the available bound electrons to be captured. The electron capture rate increases with increasing electron number density. In summary, the decay rate of ^{205}Pb is sensitive to temperature and electron density. To study the abundance ratio of ^{205}Pb/^{205}Tl in the early solar system, it is necessary to consider the influence of the environment on the decay.

IV. SUMMARY

In this study, we developed a comprehensive framework for calculating the effective decay rates of nuclei in astrophysical environments, incorporating the effects of temperature, electron number density, ionization, and nonthermal equilibrium. Using ^{26}Al as a case study, we addressed the challenge of incomplete thermal equilibrium due to large spin differences in internal γ-transitions

Table 4. Log ft values for the decay of ^{79}Se$\rightarrow^{79}$Br.

Transitions	Log ft
g.s.$\rightarrow$g.s.	10.8
0.096 MeV$\rightarrow$g.s.	4.7 [25]

Table 5. Log ft values for the decay of ^{205}Pb$\rightarrow^{205}$Tl.

Transitions	Log ft
g.s.$\rightarrow$g.s.	12 [7]
0.00232 MeV$\rightarrow$g.s.	5.91 [27]
0.262 MeV$\rightarrow$g.s.	6.5 [7]

between the isomer (0^+) and ground state (5^+). This extends the work of Takahashi and Yokoi [7] by providing a more nuanced understanding of nuclear decay in stellar environments. We also calculated the effective decay rates of ^{59}Fe, ^{79}Se, and ^{205}Pb using the latest experimental data. Our results demonstrate that these decay rates vary significantly under the influence of astrophysical conditions, with particular sensitivity to temperature and electron density.

Notably, we found that the inclusion of electron number density in the decay rate calculation for ^{59}Fe, a factor overlooked by Gao [21], provides a more accurate representation of its astrophysical behavior. These findings have important implications for nucleosynthesis models. For instance, the yield ratio of ^{60}Fe/^{26}Al is significantly altered when environmental effects are considered. Furthermore, our results highlight the sensitivity of branching ratios in the s-process to astrophysical conditions, offering new insights into elemental abundance patterns.

In conclusion, our study underscores the importance of considering astrophysical environmental effects on nuclear decay rates, providing new insights into the origin of elements and constructing astrophysical nucleosynthesis. Future studies should extend this framework to other nuclei and explore additional environmental factors, such as magnetic fields and nonthermal equilibrium. Such studies will further refine our understanding of stellar evolution and the origin of elements in the universe.

References

[1] A. G. W. Cameron, Astrophys. J. **130**, 452 (1959)
[2] J. N. Bahcall, Astrophys. J. **139**(1), 318 (1964)
[3] V. L. Peterson and J. N. Bahcall, Astrophys. J. **138**, 437 (1963)
[4] G. M. Fuller, W. A. Fowler and M. J. Newman, Astrophys. J. Suppl **42**, 447 (1980)
[5] S. Liu, C. Gao and C. Xu, Phys. Rev. C **104**, 024304 (2021)
[6] D. Mascali, D. Santonocito, G. de Angelis, *et al*, Front. Astron. Space Sci **9**, 1087543 (2022)
[7] K. Takahashi and K. Yokoi, At. Data Nucl. Data Tables

36(3), 375 (1987)
[8] R. A. Ward and W. A. Fowler, Astrophys. J. **5**, 238 (1980)
[9] A. Coc, M. G. Porquet and F. Nowacki, Phys. Rev. C **61**, 015801 (1999)
[10] K. A. Li, Y. H. Lam, C. Qi *et al*., Phys. Rev. C **94**, 065807 (2016)
[11] J. P. Cox and R. T. Giuli. Principles of Stellar Structure. First edition. (New York: Gordon and Breach, Science Publishers, Inc., 1968), p. 107.
[12] T. Oda, M. Hino, K. Muto *et al*., Atom Data Nucl Data **56**(2), 231 (1994)
[13] S. Liu and C. Xu. Chin, Phys. C **46**(5), 054106 (2022)

[14] K. Langanke and G. Martınez-Pinedo, Nucl. Phys. A **673**(1), 481 (2000)

[15] E. J. Konopinski and G. E. Uhlenbeck, Phys. Rev. **60**, 308 (1941)

[16] J. P. Davidson, Phys. Rev. **82**, 48 (1951)

[17] K. Takahashi and K. Yokoi, Nucl. Phys. A **404**(3), 578 (1983)

[18] A. Gupta, C. Lahiri and S. Sarkar, Phys. Rev. C **100**, 064313 (2019)

[19] Z. Chen, L. Rosenberg and L. Spruch, Phys. Rev. A **35**, 1981 (1987)

[20] F. Salvat, J. M. Fernández-Varea and W. Williamson, Comput. Phys. Commun. **90**(1), 151 (1995)

[21] B. Gao, S. Giraud, K. A. Li *et al*., Phys. Rev. Lett. **126**, 152701 (2021)

[22] S. Woosley and A. Heger, Phys. Rep. **442**(1), 269 (2007)

[23] R. C. Runkle, A. E. Champagne and J. Engel, Astrophys. J. **556**(2), 970 (2001)

[24] Li, K., Lam, Y.H., Qi, C. *et al*, Eur. Phys. J. C. **109**, 04006 (2016)

[25] N. Klay and F. Käppeler, Phys. Rev. C **38**, 295 (1988)

[26] R. Baker, M. Schönbächler, M. Rehkämper *et al*., Earth Planet. Sci. Lett **291**(1), 39 (2010)

[27] C. Dong, Z. H. Li, G. X. Li *et al*., Nucl. Phys. Rev. **41**(2), 611 (2024) (in Chinese)

[28] G. Leckenby, R. S. Sidhu, R. J. Chen *et al*., Nature **635**(1), 321 (2024)